Journal of Computational Physics 229 (2010) 6466–6484

Contents lists available at ScienceDirect

Journal of Computational Physics

journal homepage: www.elsevier.com/locate/jcp

Dynamic simulation of locally inextensible vesicles suspended in an arbitrary two-dimensional domain, a boundary integral method

Abtin Rahimian [a], Shravan Kumar Veerapaneni [b], George Biros [a,*]

[a] School of Computational Science and Engineering, College of Computing, Georgia Institute of Technology, Atlanta, GA 30332, United States
[b] Courant Institute of Mathematical Sciences, New York University, New York, NY 10003, United States

ARTICLE INFO

Article history:
Received 12 October 2009
Received in revised form 4 April 2010
Accepted 10 May 2010
Available online 27 May 2010

Keywords:
Stokes flow
Suspensions
Particulate flows
Vesicle simulations
Boundary integral method
Fluid membranes
Semi-implicit algorithms
Fluid–structure interaction
Fast multipole methods

ABSTRACT

We consider numerical algorithms for the simulation of hydrodynamics of two-dimensional vesicles suspended in a viscous Stokesian fluid. The motion of vesicles is governed by the interplay between hydrodynamic and elastic forces. Continuum models of vesicles use a two-phase fluid system with interfacial forces that include tension (to maintain local "surface" inextensibility) and bending. Vesicle flows are challenging to simulate. On the one hand, explicit time-stepping schemes suffer from a severe stability constraint due to the stiffness related to high-order spatial derivatives in the bending term. On the other hand, implicit time-stepping schemes can be expensive because they require the solution of a set of nonlinear equations at each time step.

Our method is an extension of the work of Veerapaneni et al. [S.K. Veerapaneni, D. Gueyffier, D. Zorin, G. Biros, A boundary integral method for simulating the dynamics of inextensible vesicles suspended in a viscous fluid in 2D, Journal of Computational Physics 228(7) (2009) 2334–2353], in which a semi-implicit time-marching scheme based on a boundary integral formulation of the Stokes problem for vesicles in an unbounded medium was proposed.

In this paper, we consider two important generalizations: (i) confined flows within arbitrary-shaped stationary/moving geometries; and (ii) flows in which the interior (to the vesicle) and exterior fluids have different viscosity. In the rest of the paper, we will refer to this as the "*viscosity contrast*". These two problems require solving additional integral equations and cause nontrivial modifications to the previous numerical scheme. Our method does not have severe time-step stability constraints and its computational cost-per-time-step is comparable to that of an explicit scheme. The discretization is pseudo-spectral in space, and multistep BDF in time. We conduct numerical experiments to investigate the stability, accuracy and the computational cost of the algorithm. Overall, our method achieves several orders of magnitude speed-up compared to standard explicit schemes.

As a preliminary validation of our scheme, we study the dependence of the inclination angle of a single vesicle in shear flow on the viscosity contrast and the reduced area of the vesicle, the lateral migration of vesicles in shear flow, the dispersion of two vesicles, and the effective viscosity of a dilute suspension of vesicles.

© 2010 Elsevier Inc. All rights reserved.

* Corresponding author.
E-mail addresses: rahimian@gatech.edu (A. Rahimian), shravan@ims.nyu.edu (S.K. Veerapaneni), gbiros@acm.org, biros@seas.upenn.edu (G. Biros).

0021-9991/$ - see front matter © 2010 Elsevier Inc. All rights reserved.
doi:10.1016/j.jcp.2010.05.006

1. Introduction

Vesicles are closed lipid membranes suspended in a viscous medium. The mechanical deformation of vesicles and their interaction with viscous fluids are thought to play an important role in many biological phenomena [13,31] and are used experimentally to understand properties of biomembranes [30]. In addition, vesicle mechanics have been used as models for the motion of red and white blood cells [19,22], whose quantitative description will help in better understanding blood rheology.

In this article, we focus on numerical schemes for continuum models of vesicle dynamics. This is a challenging problem because the motion and shape of the vesicles must be determined dynamically from a balance of interfacial forces with fluid stresses. The shape dynamics of fluid vesicles is governed by the coupling of the flow within the membrane of the vesicle with the hydrodynamics of the surrounding bulk fluid. Following our previous work on vesicle flows [34], we present a semi-implicit numerical scheme for the simulation of the motion of arbitrarily shaped vesicles that can have a viscosity contrast with the background fluid. We also extend our formulation to handle interior flows and interaction of vesicles with other moving particles with prescribed motion.

Our method is based on an integral equation formulation. In particulate flow problems involving vesicles, the elastic and incompressibility properties of their membranes must be resolved and the numerical schemes must be modified in order to accommodate these properties and to solve the resulting set of equations. Details of the boundary integral formulation for elastic interfaces and incompressible vesicles can be found in the works of Pozrikidis [24,25].

The overwhelming majority of works on particulate flows uses explicit schemes that pose severe restrictions on the time step. In contrast, semi-implicit methods result in two to three orders of magnitude larger step size that is almost independent of the spacial grid size [34]. In contrast to stencil-based methods (e.g. finite element methods), integral equation formulations avoid discretization of the overall domain and instead discretize only the vesicle-boundary and the boundary of the enclosing domain. This is the main reason that integral equations have been used extensively for vesicle, and more generally, particulate and interfacial flow simulations [25].

1.1. Contributions

The boundary integral formulation coupled to the shape dynamics results in an integro-differential equation that is constrained by the local inextensibility. Extending our previous work [34], we use semi-implicit time-stepping, fast summation schemes, and spectral discretization in space. The combination of these approaches for flows with interface singularities is not unique. However, we are unaware of any previous analysis and application of implicit time-stepping schemes combined with fast solvers to vesicles that have a viscosity contrast with the surrounding fluid and are interacting with confined boundaries. These improvements enable the simulation a large number of interacting vesicles, as described in Sections 3 and 4, and depicted in Fig. 1.

The main contributions of this paper are:

- The extension of the techniques developed in [14,20,34] to vesicle flows in confined geometry and vesicles with viscosity contrast.
- The numerical investigation of the stability and accuracy of the time-stepping schemes.
- A preliminary validation of our methodology by comparing our numerical results to results in the literature.

In particular, for validation, we investigate (i) the dependence of vesicles' inclination angle in shear flow on viscosity contrast and reduced area; (ii) the lateral migration of vesicles in shear flow due to collision; and (iii) the rheology of a dilute suspension of vesicles.

1.2. Limitations

The most significant limitation of our method is that the number of Fourier modes used to represent the vesicle membrane and the time step are not chosen adaptively. The former is a minor limitation (in 2D) but the latter is quite significant. Our spectral discretization (which we combine with a special high-order scheme for singular integrals) in space [34] results in discretization errors that are dominated by the time-stepping scheme. In our experiments, 64–128 Fourier modes in space are typically sufficient to fully resolve the shapes of the vesicles in the flow regimes we have examined. For more concentrated suspensions, adaptive schemes combined with a posteriori estimates may be necessary.

We solve the discretized system of equations using the Generalized Minimum Residual Method (GMRES) [29] with an appropriate set of preconditioners, which are based on the spectral properties of the operators. Nonetheless, for very small viscosity contrasts $\nu \ll 1$ (see Table 1 for its definition), the spectral properties of the operators change and a generic preconditioner, as we use here, fails to fully compensate for the poor conditioning of the operators.

1.3. Related work

Vesicles are used, theoretically and experimentally, to investigate the properties of biological membranes [30], blood cells [19,22], and drug-carrying capsules [32].

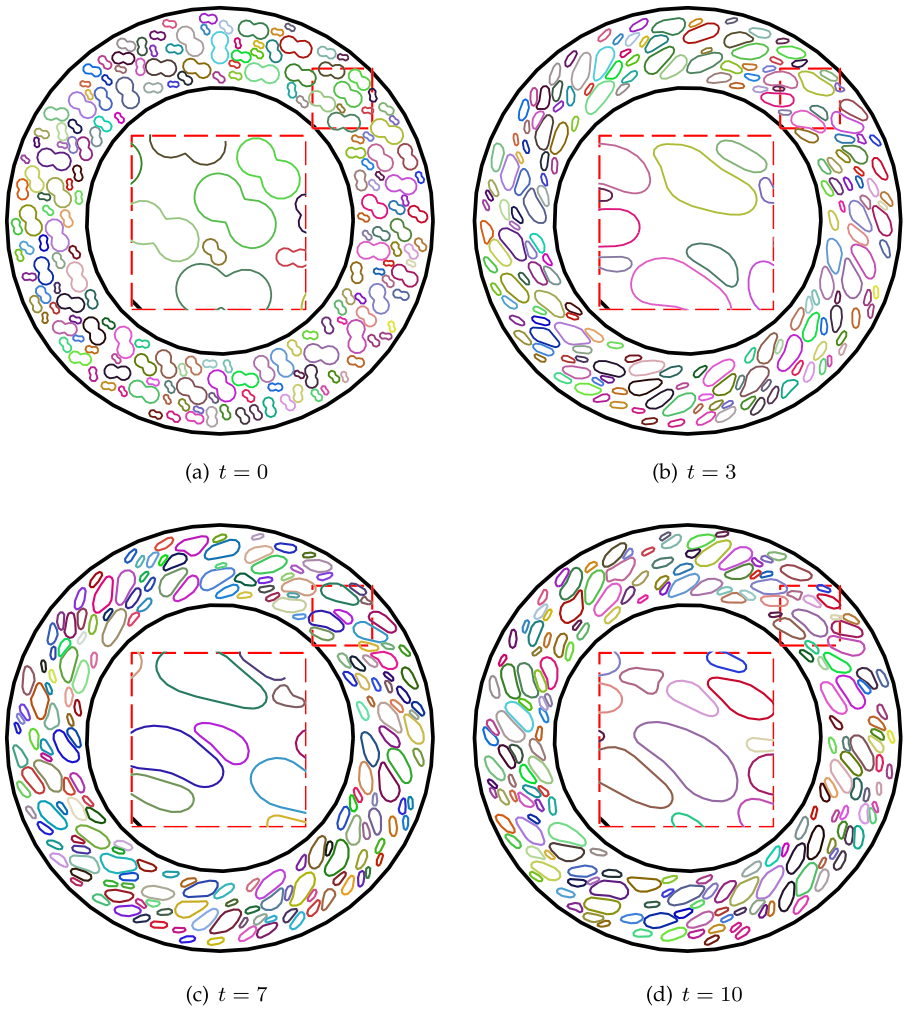

(a) $t = 0$ (b) $t = 3$

(c) $t = 7$ (d) $t = 10$

Fig. 1. In this figure, we demonstrate the capabilities of our method; in particular, its ability to resolve complex interactions between multiple vesicles. We simulated the motion of 192 vesicles in a 2D Couette apparatus. The outer boundary is fixed while the inner boundary rotates with a constant angular velocity. In this simulation, we used 64 discretization points per vesicle, 640 points on boundaries, and we took a total of 1000 time steps. The computations were performed using MATLAB. The wall-clock time per time-step is 80 s on a Xeon processor, vesicle–vesicle and vesicle–boundary interactions are evaluated on a NVIDIA Tesla Graphics Processing Unit with the total wall-clock time being three seconds per time-step. Four snapshots of the simulation are shown. We zoom in on the region marked by the broken-line square to show the details of the interaction between vesicles. Here, $t \in [0,10]$ is the nondimensional time. In this time span, the inner cylinder makes approximately one full rotation. The initial configuration was obtained by random distribution of vesicles. Due to bending, the vesicle shapes are quickly smoothed to lower energy configurations. We resolve high curvature regions (subfigures (c) and (d)), conserve vesicle areas and lengths ($\max|A - A_0|/A_0 = 2.18\text{e}-2$ and $\max|L - L_0|/L_0 = 4.69\text{e}-2$), and compute the hydrodynamic interactions with sufficient accuracy to avoid collisions without employing a collision detection algorithm. Details on the accuracy and complexity of our method are presented in later sections.

Integral equation methods have been used extensively for the simulation of Stokesian particulate flows, mostly for droplets (with or without viscosity contrast) and bubbles. These methods were introduced by Youngren and Acrivos [38] for a flow past a rigid particle of arbitrary shape. An excellent review of numerical methods for Stokesian flows is done by Pozrikidis [25]. The present work is based on a formulation derived by Rallison and Acrivos [27] for two fluids separated by an interface with surface forces and the work of Power et al., who, in a series of papers [20,21], introduced an integral equation formulation of the Stokes problem on a multiply-connected domain with Dirichlet boundary conditions.

In spite of the large body of literature devoted to investigating the rheological properties of red blood cell and vesicles suspensions, to the best our knowledge, the work on numerical methods for vesicle flows with viscosity contrast and confined boundaries is rather limited. Freund [8] considers vesicles with no viscosity contrast in a bounded domain. In his work, the boundaries are treated as panels fixed to their location with virtual springs. Zhou and Pozrikidis [39] consider the flow of a periodic suspension of 2D viscous drops between two parallel plane walls, for which an explicit expression of Green's function is available.

Let us also mention works related to the test-case flows we have used to validate our numerical method. Kraus et al. [13] studied the dynamics of a vesicle and its steady-state inclination angle in the absence of viscosity contrast. Beaucourt et al.

Table 1
Index of frequently used symbols and operators.

Symbol	Definition	Operator	Definition
γ_p	Boundary of pth vesicle	$\mathcal{B}(\mathbf{y})\mathbf{x}$	Bending operator, Eq. (2.8)
Γ	Boundary of Ω	$\mathcal{B}[\boldsymbol{\eta},\Xi,\Lambda](\mathbf{x})$	Hydrodynamic operator due to fixed boundaries with density $\boldsymbol{\eta}$ Rotlet strength Ξ, and Stokeslet strength Λ, evaluated at point $\mathbf{x}$, Appendix A
Λ	Reduced area, Section 2.3		
ζ	Traction jump across interface, Section 2.2		
$\boldsymbol{\eta}$	Double-layer density over Γ, Appendix A		
μ	Fluid viscosity	$\mathcal{E}[\mathbf{y},\mathbf{u},\zeta](\mathbf{x})$	Hydrodynamic operator due to current configuration of vesicle $\mathbf{y}$, velocity field $\mathbf{u}$, and traction jump ζ evaluated at point $\mathbf{x}$, Eq. (2.3)
v_p	Viscosity contrast μ_p/μ_0		
σ	Tension, or stress tensor		
χ	Shear rate		
ω_p	Domain enclosed by γ_p	$\mathcal{P}(\mathbf{x})$	Surface divergence operator, Eq. (2.1c)
Ω	Domain of interest		
p	Pressure	$\mathcal{T}(\mathbf{y},\mathbf{x})\sigma$	Tension operator, Eq. (2.8)
T	Simulation time horizon		
$\mathbf{u}$	Velocity		

[5] tackled the same problem in the presence of viscosity contrast. Kantsler and Steinberg [10] reported results from experimental study of the inclination angle of vesicles and their transition from tank-treading to tumbling. Misbah [18] looked at the theoretical aspects of a vesicle's inclination angle problem. Loewenberg [15], Loewenberg and Hinch [16] studied the dispersion of drops in shear flow and Eckstein et al. [7] investigated particle–particle interaction and their lateral migration in an experimental setting. Rheology of (dilute) suspension of vesicles was investigated by Danker et al. [6], Loewenberg [15], Ramanujan and Pozrikidis [28], and Vitkova et al. [35]. Danker et al. [6] investigated the rheological properties of a dilute suspension of vesicles in shear flow analytically.

1.4. Synopsis of our method

We propose a computational scheme for the evolution of vesicles in a confined domain. The scheme builds upon our previous work [34]. We also extend our method to the case where there is a viscosity contrast between the suspending fluid and the internal fluid of the vesicle. Our scheme is based on Lagrangian tracking of marker particles on the vesicle, semi-implicit time discretization and spectral representation of the interface, together with high-order accurate quadrature rules. These choices result in a spectrally accurate method in space and second-order accurate method in time.

High-order accuracy in space is ensured by using a Fourier basis discretization for all functions and computing derivatives in Fourier domain, as well as high-order, Gauss-trapezoidal quadrature rules [1] for discretization of single-layer potentials. In time, we use a semi-implicit marching scheme [2]. This discretization yields a linear system of equations for each time step, which is solved using GMRES. One significant challenge in simulating vesicle dynamics is the numerical stiffness of the governing integro-differential equations [34]. To gain insight on the spectral properties of operators we use a "frozen coefficient" analysis on the unit circle. This analysis allows us to construct a preconditioner for the GMRES solver. Putting everything together, we were able to achieve high accuracy in space and time, while taking large time steps without incurring high computational costs. Our formulation for confined boundaries is based on the method in [20]. Finally, we resolve nearly-singular integrals, which arise when vesicles come close the fixed boundary, using the method proposed in [36].

Throughout this paper, lower case letters will refer to scalars, and lowercase bold letters will refer to vectors. We use $\otimes$ for the tensor product of two vectors and $|\cdot|$ to denote the measure of its argument (e.g. the Euclidean norm of a vector or the area of a domain). We denote the jump across interfaces by $[\![u]\!] := u^+ - u^-$, where $u^{\pm}(\mathbf{x}) := \lim_{h\downarrow 0} u(\mathbf{x} \pm h\mathbf{n})$, $\mathbf{n}$ denoting the outward normal to the boundary. We denote the convolution of an integral kernel K with density $\boldsymbol{\eta}$ by $\mathcal{K}[\mathbf{y},\boldsymbol{\eta}](\mathbf{x}) := \int_\Gamma K(\mathbf{x},\mathbf{y})\boldsymbol{\eta}(\mathbf{y})ds(\mathbf{y})$, where the product inside the integral should be interpreted as a tensor operation when K is a tensor and as a dot product when K is a vector. In Table 1, we list symbols and operators frequently used in this paper.

Finally, the rest of the paper is organized as follows: In Section 2, we state the problem and its formulation. In Section 3, we outline the numerical scheme we use to solve the derived equations. In Section 4, we report results from numerical experiments we performed to demonstrate the stability of the proposed time-marching scheme in different flow regimes and geometry configurations. In particular, we investigate the effect of fixed boundaries on the time-stepping numerical stability of our scheme. We conclude in Section 4.4 with a discussion of the rheology of dilute suspensions of vesicle flows with viscosity contrast.

2. Formulation

Consider a suspension of vesicles in an ambient Newtonian fluid. Let Ω be the domain of interest, an open bounded subset of $\mathbb{R}^2$ that can be multiply-connected and whose boundary consists of $M+1$ infinitely differentiable curves $\Gamma_0,\ldots,\Gamma_M$, among

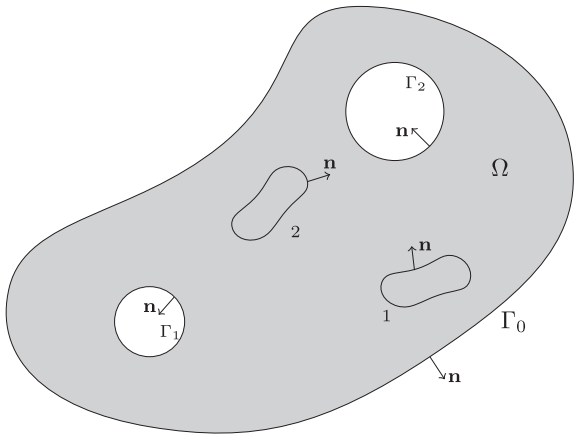

Fig. 2. A typical domain of interest Ω (shaded area) with boundary Γ_i ($i = 0,\ldots,M$). The boundary of each vesicle is denoted by γ_j ($j = 1,\ldots,N$). The enclosed domain by γ_j is denoted by ω_j.

which, Γ_0 denotes the enclosing boundary of the domain. The ambient fluid has viscosity μ_0. The vesicles are evolving under the influence of an imposed velocity field. Let $\gamma_p (p = 1,\ldots,N)$ denote the boundary of the pth vesicle, ω_p denote the domain enclosed by γ_p, and μ_p denote the viscosity of the fluid inside that vesicle (see Fig. 2). Let $\Gamma := \bigcup_k \Gamma_k$ and $\gamma := \bigcup_p \gamma_p$. We use $\mathbf{x}$ or $\mathbf{y}$ to denote both a typical point in the domain Ω and a point on the interface γ. When $\mathbf{x} \in \gamma$, we define $\dot{\mathbf{x}}$ or $\mathbf{x}_s$ as the interfacial velocity or the derivative of the $\mathbf{x}$ with respect to arc length.

When the Reynolds number is based on the vesicle size, the effect of inertial forces is insignificant and the fluid flow is governed by the Stokes equation,

$$\mu\Delta\mathbf{u} - \nabla p = \mathbf{0}, \quad \text{div } \mathbf{u} = 0, \quad \text{in } \Omega \setminus \gamma, \tag{2.1a}$$

where $\mathbf{u}(\mathbf{x},t)$ is the velocity field, $p(\mathbf{x},t)$ is the pressure field, and μ is the viscosity of fluid. We supplement (2.1a) with the velocity no-slip condition on γ_p, and with velocity Dirichlet boundary condition on Γ as

$$\mathbf{u}(\mathbf{x},t) = \dot{\mathbf{x}}(t) \quad \text{when } \mathbf{x} \in \gamma, \quad \text{and} \quad \mathbf{u}(\mathbf{x},t) = \mathbf{U}(\mathbf{x},t) \quad \text{when } \mathbf{x} \in \Gamma, \tag{2.1b}$$

where $\dot{\mathbf{x}}$, as we mentioned earlier, is the velocity of the points on the vesicle membrane. The assumption that the velocity field is continuous across the vesicle interface, $[\![\mathbf{u}]\!] = 0$, is implicit in our expression of no-slip condition. Henceforth, we drop the explicit time dependence of the variables. Finally, to enforce the local inextensibility of the vesicles we require that the surface divergence of the velocity field vanishes. That is

$$\mathbf{x}_s \cdot \mathbf{u}_s = 0 \quad \text{for } \mathbf{x} \in \gamma. \tag{2.1c}$$

Here $\mathbf{x}_s$ is the derivative of position of the points on γ with respect to arc length, i.e. the tangent vector. For notational convenience, when $\mathbf{x} \in \gamma$ and $\mathbf{u}$ is defined on γ we define $\mathcal{P}(\mathbf{x})\mathbf{u} := \mathbf{x}_s \cdot \mathbf{u}_s$; then the inextensibility condition can be written as $\mathcal{P}(\mathbf{x})\mathbf{u} = 0$ for $\mathbf{x} \in \gamma$.

2.1. Boundary integral formulation

Due to the continuity of the velocity field across the interfaces, we can follow the standard approach of potential theory [20,25,23], and reformulate Eqs. (2.1a) and (2.1b) using layer potentials. It follows that the velocity at a point $\mathbf{x}$ is formally given by

$$\alpha\mathbf{u}(\mathbf{x}) = \mathcal{E}[\mathbf{y},\mathbf{u},\boldsymbol{\zeta}](\mathbf{x}) + \mathcal{B}[\boldsymbol{\eta},\Xi,\Lambda](\mathbf{x}), \quad \mathbf{x} \in \Omega, \quad \alpha = \begin{cases} 1 & \mathbf{x} \in \Omega \setminus \cup_p \omega_p, \\ \nu_p & \mathbf{x} \in \omega_p, \\ (1+\nu_p)/2 & \mathbf{x} \in \gamma_p, \end{cases} \tag{2.2a}$$

subject to the inextensibility constraint,

$$\mathcal{P}(\mathbf{x})\mathbf{u} = 0, \quad \mathbf{x} \in \gamma, \tag{2.2b}$$

where $\nu_p := \mu_p/\mu_0$ is the contrast between the viscosity of the fluid enclosed by pth vesicle and that of the background medium, and $\boldsymbol{\zeta}$ denotes the traction jump across the interface. As it is explained in [25,23] we have

$$\mathcal{E}[\mathbf{y},\mathbf{u},\boldsymbol{\zeta}](\mathbf{x}) := \sum_{q=1}^{N} \mathcal{S}_q[\mathbf{y},\boldsymbol{\zeta}](\mathbf{x}) + \mathcal{D}_q[\mathbf{y},\mathbf{u}](\mathbf{x}). \tag{2.3}$$

Operators $\mathcal{S}_q$ and $\mathcal{D}_q$ are the single- and double-layer hydrodynamic potentials for Stokes flow evaluated on the qth interface, defined as

$$\mathcal{S}_q[\mathbf{y},\zeta](\mathbf{x}) = \frac{1}{4\pi\mu_0}\int_{\gamma_q}\left(-\log\rho I + \frac{\mathbf{r}\otimes\mathbf{r}}{\rho^2}\right)\zeta ds(\mathbf{y}), \tag{2.4}$$

$$\mathcal{D}_q[\mathbf{y},\mathbf{u}](\mathbf{x}) = \frac{1-\nu_q}{\pi}\int_{\gamma_q}\frac{\mathbf{r}\cdot\mathbf{n}}{\rho^2}\frac{\mathbf{r}\otimes\mathbf{r}}{\rho^2}\mathbf{u}ds(\mathbf{y}), \tag{2.5}$$

in which $\mathbf{r} := \mathbf{x}-\mathbf{y}$ and $\rho := |\mathbf{r}|$. $\mathcal{B}$ is the completed double-layer operator for confined Stokes flow with density $\boldsymbol{\eta}(\mathbf{y})$, defined as

$$\mathcal{B}[\boldsymbol{\eta},\Xi,\Lambda](\mathbf{x}) := \mathcal{D}[\mathbf{y},\boldsymbol{\eta}](\mathbf{x}) + \mathcal{N}_0[\mathbf{y},\boldsymbol{\eta}](\mathbf{x}) + \sum_{k=1}^{M} R(\mathbf{x},\mathbf{c}_k)\xi_k + \sum_{k=1}^{M} S(\mathbf{x},\mathbf{c}_k)\lambda_k, \tag{2.6}$$

where $\Lambda = \{\lambda_1,\ldots,\lambda_M\}$ and $\Xi = \{\xi_1,\ldots,\xi_M\}$. In Appendix A, we define $\mathcal{D}$, $\mathcal{N}_0$, R, S, Ξ, and Λ and outline the derivation of $\mathcal{B}$ that is based on [20]. Taking the limit of (2.2a) to the boundary Γ we obtain an equation for the double-layer density $\boldsymbol{\eta}$

$$\alpha\mathbf{U}(\mathbf{x}) = -\frac{1}{2}\boldsymbol{\eta}(\mathbf{x}) + \mathcal{E}[\mathbf{y},\mathbf{u},\zeta](\mathbf{x}) + \mathcal{B}[\boldsymbol{\eta},\Xi,\Lambda](\mathbf{x}) \quad \mathbf{x}\in\Gamma. \tag{2.7}$$

Operator $\mathcal{E}$ represents the velocity induced by the evolution of the vesicle and operator $\mathcal{B}$ corresponds to the velocity due to the imposed flow via the boundary Γ. Note that if we replace $\mathcal{B}$ with a far field $\mathbf{u}^\infty$ in Eq. (2.2a), we obtain the formulation for the case of an unbounded flow. Also, no that we need the traction jump ζ to evaluate $\mathcal{E}$. We give details on how to calculate the traction jump in the following section.

2.2. Traction jump across the interface

In the absence of gravity,[1] the traction jump across the interface depends exclusively on the material properties and the configuration of the interface. The traction jump across the interface balances the forces caused by bending and tension [26]. We can write $\zeta = \mathbf{f}_b + \mathbf{f}_\sigma$, where $\mathbf{f}_b$ denotes the bending force and $\mathbf{f}_\sigma$ is the force due to tension. Let κ_b denote the bending modulus of the vesicle, σ the tension, and κ the local curvature. Then, the elastic energy of the membrane is given by $\varepsilon_p(\kappa,\sigma) = \int_{\gamma_0}(\frac{1}{2}\kappa_b\kappa^2+\sigma)ds$. The forces are obtained by taking the gradient of the membrane energy. See [25,34] for details on the derivation of the expressions for these forces. Accordingly, forces can be written as $\mathbf{f}_b = -\kappa_b\mathbf{x}_{ssss}$ and $\mathbf{f}_\sigma = (\sigma\mathbf{x}_s)_s$, were the subscript s denotes differentiation with respect to arc length. For convenience, we introduce the following notation:

$$\begin{aligned}
&\mathcal{B}(\mathbf{y})\mathbf{x} = -\kappa_b\mathcal{S}[\mathbf{y},\mathbf{x}_{ssss}](\mathbf{x}),\\
&\mathcal{T}(\mathbf{y},\mathbf{x})\sigma = \mathcal{S}[\mathbf{y},(\sigma\mathbf{x}_s)_s](\mathbf{x}),\\
&\mathcal{L}(\mathbf{x}) = \mathcal{P}(\mathbf{x})\mathcal{T}(\mathbf{x},\mathbf{x}),\\
&\mathcal{M}(\mathbf{x}) = \mathcal{T}(\mathbf{x},\mathbf{x})\mathcal{L}^{-1}(\mathbf{x})\mathcal{P}(\mathbf{x}),\\
&\mathcal{D}(\mathbf{y})\mathbf{u} = \mathcal{D}[\mathbf{y},\mathbf{u}](\mathbf{x}),
\end{aligned} \tag{2.8}$$

and $\mathcal{T}(\mathbf{x}) := \mathcal{T}(\mathbf{x},\mathbf{x})$.

2.3. Scaling

Let $\bar{r}$, and $\bar{t}$ denote the characteristic length and time and let L be the perimeter of the vesicle. We define $\bar{r} := L/2\pi$ as the radius of the circle with perimeter L, and the time scale $\bar{t} := \mu_0\bar{r}^3/\kappa_b$. We define the characteristic tension as $\bar{\sigma} := \kappa_b/\bar{r}$. For the velocity scale, we consider two cases: an unbounded shear flow and a confined flow. *Shear flow*. We assume that $\mathbf{u}^\infty = \chi[x_2,0]^T$, where χ is the shear rate. The characteristic shear rate is then $\bar{\chi} := 1/\bar{t}$ and the characteristic velocity is $\bar{r}\bar{\chi}$. *Confined flow*. In this case, the characteristic velocity may be defined by $\overline{U}$ as the velocity defined on the boundary.

A parameter that determines the behavior of vesicles significantly is the *reduced area*, which is the contrast of vesicle's area to that of a circle with the same perimeter, $\Delta := A/(\pi\bar{r}^2)$.

2.4. Summary of the vesicles' equations of motion

Incorporating the notation introduced in (2.8), for a Lagrangian point $\mathbf{x}$ we can write the governing equations as

[1] We can include gravity by adding $(\Delta\rho)(\mathbf{g}\cdot\mathbf{x})\mathbf{n}$ to the traction jump, where $\Delta\rho = \rho_{\text{out}} - \rho_{\text{in}}$ is the density difference.

$$\text{Vesicle evolution}: \quad \alpha\mathbf{u}(\mathbf{x}) = \sum_{q=1}^{N} \mathcal{B}_q(\mathbf{y})\mathbf{x} + \mathcal{T}_q(\mathbf{y})\sigma + \mathcal{D}_q(\mathbf{y})\mathbf{u} + \mathcal{B}[\boldsymbol{\eta}, \Xi, \Lambda](\mathbf{x}), \quad \mathbf{x} \in \gamma, \tag{2.9a}$$

$$\text{Inextensibility constraint}: \quad \mathcal{P}(\mathbf{x})\mathbf{u} = 0, \quad \mathbf{x} \in \gamma, \tag{2.9b}$$

$$\text{Fixed boundaries}: \quad \alpha\mathbf{U}(\mathbf{x}) = -\frac{1}{2}\boldsymbol{\eta}(\mathbf{x}) + \mathcal{E}[\mathbf{y}, \mathbf{u}, \zeta](\mathbf{x}) + \mathcal{B}[\boldsymbol{\eta}, \Xi, \Lambda](\mathbf{x}), \quad \mathbf{x} \in \Gamma, \tag{2.9c}$$

These equations are solvable for the interfacial velocity and tension, as well as double-layer density $\boldsymbol{\eta}$ on the fixed boundaries.

3. Numerical algorithm

We use a multistep time-marching scheme. In Section 3.1, we give the details of our time-stepping schemes and in Section 3.2, we outline our approach to spatial discretization. Following [34], we adopt a Lagrangian formulation, which simplifies the implementation of the high-order multistep schemes.

3.1. Time discretization

We use backward difference formula (Appendix C) to advance in time, a generic form of which can be written as $\mathbf{u}^{n+1} = \frac{1}{\Delta t}(\beta\mathbf{x}^{n+1} - \mathbf{x}^o)$, in which $\mathbf{x}^o$ is a linear combination previous time steps and β depends on the order. Then, a semi-implicit formulation of equation set (2.9c) can be written as

$$\begin{aligned}\frac{\alpha}{\Delta t}(\beta\mathbf{x}^{n+1} - \mathbf{x}^o) = {} & \mathcal{B}_p(\mathbf{y}^e)\mathbf{x}^{n+1} + \mathcal{T}_p(\mathbf{y}^e)\sigma^{n+1} + \mathcal{D}_p(\mathbf{y}^e)\mathbf{u}^{n+1} + \mathcal{B}[\boldsymbol{\eta}^n, \Xi^n, \Lambda^n](\mathbf{x}^e) \\ & + \sum_{\substack{q=1 \\ q\neq p}}^{N} \left\{\mathcal{B}_q(\mathbf{y}^e)\mathbf{x}^n + \mathcal{T}_q(\mathbf{y}^e)\sigma^n + \mathcal{D}_q(\mathbf{y}^e)\mathbf{u}^n\right\}, \quad \mathbf{x} \in \gamma_p\end{aligned} \tag{3.1a}$$

$$\beta\mathcal{P}(\mathbf{y}^e)\mathbf{x}^{n+1} = \mathcal{P}(\mathbf{y}^e)\mathbf{x}^o =: g, \tag{3.1b}$$

$$\alpha\mathbf{U}(\mathbf{x}) = -\frac{1}{2}\boldsymbol{\eta}^{n+1}(\mathbf{x}) + \mathcal{E}[\mathbf{y}^{n+1}, \mathbf{u}^{n+1}, \zeta^{n+1}](\mathbf{x}) + \mathcal{B}[\boldsymbol{\eta}^{n+1}, \Xi^{n+1}, \Lambda^{n+1}](\mathbf{x}) \quad \mathbf{x} \in \Gamma, \tag{3.1c}$$

where, $\mathbf{y}^e$ is the interfacial position obtained by extrapolation form previous locations (see Appendix C). We will use g to denote the right-hand side of (3.1b). Γ is fixed or has a prescribed motion; $\mathbf{U}$ may depend on time. We would like to make the following remarks regarding our scheme:

- The vesicle-boundary interactions are treated explicitly.
- The vesicle-vesicle interactions are also explicit.
- For each vesicle, its new position and tension are computed semi-implicitly by solving a *linear* system of equations.

Algorithm 1. Semi-implicit time-marching.

Require: $E^n_{\text{far}}, g, \mathbf{q}$

//Solving (3.6) for the vesicle

for p = 1 to N **do**

$\sigma_{\text{exp}} \leftarrow \mathcal{L}_p\sigma^{n+1}_{\text{exp}} = \alpha g - \mathcal{P}\mathbf{q}$ //Calculating the tension part of the RHS

$\mathbf{r} \leftarrow \mathbf{q} + \mathcal{T}_p\sigma^{n+1}_{\text{exp}}$

$\mathbf{x}^{n+1} \leftarrow$ use GMRES to solve (3.6) with right-hand side $\mathbf{r}$ and $\mathbf{x}^e$ as initial guess.

$\sigma_{\text{imp}} \leftarrow \mathcal{L}_p\sigma^{n+1}_{\text{imp}} = -\mathcal{P}(\beta\mathcal{D}_p + (\Delta t)\mathcal{B}_p)\mathbf{x}^{n+1}$ //Solving for σ in (3.5) with known position $\mathbf{x}^{n+1}$

$\sigma^{n+1} \leftarrow (\sigma^{n+1}_{\text{exp}} + \sigma^{n+1}_{\text{imp}})/(\Delta t)$

end for

$\mathbf{u}^{n+1} \leftarrow \frac{1}{\Delta t}(\beta\mathbf{x}^{n+1} - \mathbf{x}^o)$

$\zeta^{n+1} \leftarrow \kappa_b\mathbf{x}^{n+1}_{ssss} + (\sigma^{n+1}\mathbf{x}^{n+1}_s)_s$ //Solving (3.1c) for double-layer density $\boldsymbol{\eta}$

$\mathbf{r} \leftarrow \alpha\mathbf{U} - \mathcal{E}[\mathbf{x}^{n+1}, \mathbf{u}^{n+1}, \zeta^{n+1}]$

$\boldsymbol{\eta}^{n+1} \leftarrow (-I/2 + \mathcal{B})^{-1}\mathbf{r}$ //The inverse can be precomputed

return $\mathbf{x}^{n+1}$, σ^{n+1}, $\boldsymbol{\eta}^{n+1}$

To advance in time, first we need to solve the coupled system of Eqs. (3.1a) and (3.1b) to calculate the new position of the vesicle $\mathbf{x}^{n+1}$ and tension σ^{n+1}. Then, we solve (3.1c) to calculate $\boldsymbol{\eta}^{n+1}$. We explore two different schemes to solve (3.1a) and (3.1b).

3.1.1. Semi-implicit scheme

Let

$$E^n_{\text{far}} := \sum_{\substack{q=1 \\ q\neq p}}^{N} \{\mathcal{B}_q(\mathbf{y}^e)\mathbf{x}^n + \mathcal{T}_q(\mathbf{y}^e)\sigma^n + \mathcal{D}_q(\mathbf{y}^e)\mathbf{u}^n\} + \mathcal{B}[\boldsymbol{\eta}^n, \Xi^n, \Lambda^n](\mathbf{x}^e), \quad \mathbf{x} \in \gamma_p \tag{3.2}$$

Then, we rewrite (3.1a) as

$$\frac{\alpha}{\Delta t}(\beta\mathbf{x}^{n+1} - \mathbf{x}^o) = \mathcal{B}_p(\mathbf{y}^e)\mathbf{x}^{n+1} + \mathcal{T}_p(\mathbf{y}^e)\sigma^{n+1} + \mathcal{D}_p(\mathbf{y}^e)\mathbf{u}^{n+1} + E^n_{\text{far}}. \tag{3.3}$$

Upon rearranging, we obtain

$$[\alpha\beta I - \beta\mathcal{D}_p - (\Delta t)\mathcal{B}_p]\mathbf{x}^{n+1} - (\Delta t)\mathcal{T}_p\sigma^{n+1} = \mathbf{q}, \tag{3.4}$$

where $\mathbf{q} := (\alpha I - \mathcal{D}_p)\mathbf{x}^o + E^n_{\text{far}}$ (for brevity, we have dropped the notational dependence of the operators on $\mathbf{y}^e$). Notice that

$$\alpha\beta\mathbf{x}^{n+1} = (\beta\mathcal{D}_p + (\Delta t)\mathcal{B}_p)\mathbf{x}^{n+1} + (\Delta t)\mathcal{T}_p\sigma^{n+1} + \mathbf{q}.$$

Substituting into (3.1b), we get an equation for tension as a function of the vesicle's configuration,

$$(\Delta t)\mathcal{L}_p\sigma^{n+1} = \alpha g - \mathcal{P}\mathbf{q} - \mathcal{P}(\beta\mathcal{D}_p + (\Delta t)\mathcal{B}_p)\mathbf{x}^{n+1}. \tag{3.5}$$

Substituting this in (3.4), the equation for the new position is

$$\{\alpha\beta I + (\mathcal{M}_p - I)(\beta\mathcal{D}_p + (\Delta t)\mathcal{B}_p)\}\mathbf{x}^{n+1} = \mathbf{q} + \mathcal{T}_p\mathcal{L}_p^{-1}(\alpha g - \mathcal{P}\mathbf{q}). \tag{3.6}$$

Algorithm 2. Explicit time-marching.

Require: $E^n_{\text{far}}, g, \mathbf{q}$
  for $p = 1$ to N **do**
    $\mathbf{r} \leftarrow \mathbf{q} + (\Delta t)\mathcal{T}_p\sigma^n$
    $\mathbf{x}^{n+1} \leftarrow$ update position using (3.7)
    $\sigma^{n+1} \leftarrow$ solve for tension using (3.8)
  end for
  $\mathbf{u}^{n+1} \leftarrow \frac{1}{\Delta t}(\beta\mathbf{x}^{n+1} - \mathbf{x}^o)$
  $\zeta^{n+1} \leftarrow \kappa_b\mathbf{x}^{n+1}_{ssss} + \left(\sigma^{n+1}\mathbf{x}^{n+1}_s\right)_s$
  `//Solving (3.1c) for double-layer density` $\boldsymbol{\eta}$
  $\mathbf{r} \leftarrow \alpha\mathbf{U} - \mathcal{E}[\mathbf{x}^{n+1}, \mathbf{u}^{n+1}, \zeta^{n+1}]$
  $\boldsymbol{\eta}^{n+1} \leftarrow (-I/2 + \mathcal{B})^{-1}\mathbf{r}$
  return $\mathbf{x}^{n+1}$, σ^{n+1}, $\boldsymbol{\eta}^{n+1}$

3.1.2. Explicit scheme

Let E^n_{far} be defined as before. Another approach is to first calculate $\mathbf{x}^{n+1}$ explicitly and then compute the corresponding σ^{n+1}. Therefore, (3.4) can be written as

$$\alpha\beta\mathbf{x}^{n+1} = (\Delta t)\mathcal{T}_p\sigma^n + \mathbf{q} + (\beta\mathcal{D}_p + \Delta t\mathcal{B}_p)\mathbf{x}^e. \tag{3.7}$$

Accordingly, the equation for tension becomes

$$(\Delta t)\mathcal{L}_p\sigma^{n+1} = \alpha g - \mathcal{P}\mathbf{q} - \mathcal{P}(\beta D_p + \Delta t\mathcal{B}_p)\mathbf{x}^{n+1}. \tag{3.8}$$

In Algorithms 1 and 2, we give the pseudocode for our numerical schemes.

3.2. Spatial discretization

Let $\theta \in (0, 2\pi]$ be a parametrization of the interface γ_p and $\theta_k = 2k\pi/n$ ($k = 1, \ldots, n$) be n uniformly distributed discretization points. We have

$$\mathbf{x}(\theta) = \sum_{k=-n/2+1}^{n/2} \hat{\mathbf{x}}(k)e^{-ik\theta}.$$

This enables us to use FFT to calculate $\hat{\mathbf{x}}$ and derivatives of $\mathbf{x}$ with spectral-accuracy, since we have assumed that γ and Γ belong to C^∞.

3.2.1. Quadrature rule

The single-layer potential $\mathcal{S}$ has a logarithmic singularity. For its integration, we use the hybrid Gauss-trapezoidal quadrature rule given in Table 8 of [1], designed to handle this kind of singularity. Let $\mathbf{y}_k = \mathbf{y}(\theta_k)$, then

$$\mathcal{S}[\mathbf{y},\zeta](\mathbf{x}) \approx \sum_{k=1}^{n+m} w_k S(\mathbf{x},\mathbf{y}_k)\zeta(\mathbf{y}_k)|\mathbf{y}_{\theta,k}|,$$

where n is the number of nodes, m is number of quadrature nodes, w_k the quadrature weights, and $\mathbf{y}_\theta$ is the Jacobian. The number m is determined by the desired order of convergence for the integral.

The double-layer potential has no singularity in two dimensions and for $\mathbf{x},\mathbf{y} \in \gamma$, $\lim_{\mathbf{x}\to\mathbf{y}} D(\mathbf{x},\mathbf{y}) = \kappa \mathbf{t}\otimes\mathbf{t}/2\pi$. Thus, a composite trapezoidal rule will give spectral-accuracy since the integrands are periodic and smooth. Therefore,

$$\mathcal{D}[\mathbf{y},\mathbf{u}](\mathbf{x}) \approx \frac{2\pi}{n}\sum_{k=1}^{n} D(\mathbf{x},\mathbf{y}_k)\mathbf{u}(\mathbf{y}_k)|\mathbf{y}_{\theta,k}|.$$

3.3. Analysis of the spectral properties

We use spectral analysis of the operators defined on the unit circle to characterize the stiffness of the underlying problem. If we use n Lagrangian points to represent the interface, as it is explained in detail in [34], the condition number of the single-layer potential operator scales as $O(n)$ and the condition number of the bending operator scales as $O(n^3)$. On the other hand, the double-layer potential operator alters only the first three frequencies of the integrand.

The coefficient $\alpha = \frac{1+\nu_q}{2}$ and the operator $\mathcal{D}$, given in (2.5). Now, consider three cases where $\nu \gg 1$, $\nu \approx 1$, and $\nu \ll 1$: (i) $\nu \gg 1$: the vesicle acts more like a rigid body and in (3.6), $\frac{1}{\alpha}\mathcal{D}$ remains finite but $\frac{1}{\alpha}\mathcal{B}$ tends to zero and thus the double-layer operator dominates. Therefore, the condition number of the whole operator is bounded. (ii) $\nu \approx 1$: the effect of double-layer potential is minimal and the bending operator dominates. (iii) $\nu \ll 1$: the double-layer potential and bending terms are comparable to each other. In the last two cases, the condition number of the operator grows in cubic rate thereby requiring preconditioning for the iterative solvers. We explore this in greater detail in our experiments in Section 4.1. The existence of viscosity contrast has no effect on the tension operator and thus its spectral properties are the same as those explored in [34].

In our time-stepping scheme, we require the solution of systems with the operators $\mathcal{L}$, and $I + (\mathcal{M} - I)(\mathcal{D} + (\Delta t)\mathcal{B})$. Based on our spectral analysis here and in [34], the condition number of these system behave as $O(n)$ and $O(n^3)$, where n is the number of modes in space. In [34], we proposed a set of low-cost preconditioners for the position and tension solver. Since the tension operator is exactly the same for all cases of viscosity contrast, what we had for the case of $\nu = 1$ carries over to the general case. On the other hand, because the double-layer operator has a bounded condition number, the main source of ill-conditioning for the position solver (at least at moderate values of viscosity contrast) is the bending operator and the preconditioner proposed in [34] applies.

3.4. Computational cost of the semi-implicit scheme for a single time-step

Assume that we have N vesicles, with n discretization points per vesicle interface and m discretization points on the boundary Γ (in the case of bounded flow, of course). The semi-implicit scheme involves "inversion" of three operators: the prescribed-motion boundary double-layer, the inextensibility operator, and the position-update operator. And it also requires evaluation of single- and double-layers, and differentiations on the vesicle-boundary.

The semi-implicit algorithm has two main components: one is the evaluation of the effect of boundaries on a vesicle's Lagrangian points and the other is the solution of (3.6) for the new position and tension. The are two facts that lead to a fast algorithm: (1) the double-layer operator is well-conditioned and thus, GMRES converges to the solution in mesh-independent manner;and (2) the boundary-vesicle and vesicle-vesicle interactions can be accelerated by the fast multipole method. Thus, using GMRES, the calculation of the density over Γ requires $O(m)$ work per time step.[2] The evaluation the double-layer at each Lagrangian point on the vesicle interface (evaluation of $\mathcal{B}$) is $O(m)$ and, using FMM, $O(Nn+m)$ for all vesicles.[3] Furthermore, we use FFT to calculate the derivatives, thus the evaluation of traction jump on each vesicle requires $O(n\log n)$ per time step. When we solve for the positions using (3.6), at each GMRES iteration of position, we solve for tension, which takes $O(Nn\log n)$ time and thus, each GMRES iteration requires $O(Nn\log n)$ work. However, in Section 4.1, we demonstrate numerically that the number of iterations is nearly independent of the problem size (Table 4). Hence, the overall cost of updating the positions and the tensions for all vesicles is $O(Nn\log n + m)$.

[2] Alternatively, when the boundary with prescribed motion is fixed, one could use a fast scheme to precompute the action of its inverse to a vector [17].

[3] Notice, that when the number of vesicles is high, one needs to implement a fast summation scheme for the Rotlet and Stokeslet terms. The Kernel Independent Fast Multipole Method can be used for this purpose [37].

4. Numerical experiments

In this section, we present results on the convergence, stability, and algorithmic complexity of the proposed methods, which we have implemented in MATLAB. We preform the following tests:

- We consider a single vesicle in Section 4.1. Our goal is to demonstrate the stability and accuracy of our scheme as a function of the parameters, specifically viscosity contrast v. We also report the dependence of tank-treading inclination angle on a vesicle's viscosity contrast and shear rate.
- We consider the dispersion of vesicles due to pairwise interaction and collision in shear flow is studied in Section 4.2.
- We consider the effect of fixed boundaries in Section 4.3 and their effect on the overall accuracy of our method.
- We consider the rheological properties of dilute suspensions of vesicles in Section 4.4.

4.1. Single vesicle

We consider the case of a single vesicle with viscosity contrast v suspended in an unbounded shear flow. In our experiment, we consider v to be 0.01, 0.1, 1, 10, and 100. When the viscosity contrast is low, based on experiment and theory [10,18], the vesicle undergoes a tank-treading motion at an equilibrium angle ϕ_v. When the viscosity contrast is high, the vesicle tumbles. We first investigate the stability and convergence properties of the proposed numerical schemes. In Table 2, we report the largest uniform step-size required to maintain numerical stability for different shear rates and viscosity contrasts for a BDF method of order two for the semi-implicit time-marching scheme (we used a simple bisection method to find these time steps). The time horizon is chosen such that the vesicle reaches steady-state or the desired dynamical phenomenon (i.e. tank-treading or tumbling is observed). The reduced area Δ is set to .4 and .75. Comparing these results with the results of the explicit scheme given in Table 3, we see three orders of magnitude speed-up for most cases. In Figs. 3, and 4, we show the configuration of the vesicle for different values of viscosity contrasts v and reduced area Δ. In Fig. 5, we show the sedimentation shape of the vesicle under the influence of gravity.

In Table 4, we report the number of GMRES iterations (corresponding to $\Delta = .75$ only). Observe that the number of iterations for the tension solver is almost mesh-independent and viscosity contrast has no effect on the tension solver, as expected. The effect of the high condition number (caused by bending) becomes very pronounced in cases where the mesh size equals 128 and 256 but our preconditioner compensates for that well.

Due to inextensibility and incompressibility, the length and area of vesicles should be preserved. In Table 5, we report the relative error in area and length of a single vesicle in shear flow.

The inclination angle of vesicles in tank-treading motion is of physical interest since it can be compared with experimental results. Since we consider only two-dimensional vesicle flows, this comparison is qualitative. Based on theory, this inclination angle depends only on the reduced area Δ and the viscosity contrast v. For any fixed Δ, there exists a v_c such that for

Table 2
Stable step size for a second-order semi-implicit scheme. The initial vesicle configuration is the same as the one given in Fig. 3. When $\chi = 0$, the vesicle relaxes to minimum energy equilibrium shape. Since there is no input energy from the ambient fluid flow, all step sizes are permissible and do not lead to (numerical) instability. Comparing with Table 3, we see three orders of magnitude speed-up.

n	$v = .01$		$v = .1$		$v = 1$		$v = 10$		$v = 100$	
	$\chi = 1$	10	1	10	1	10	1	10	1	10
$\Delta = .4$										
32	4e−1	2e−2	2e−1	1e−2	2e−1	7e−2	7e−1	9e−2	7e−1	7e−2
64	4e−1	1e−2	2e−1	1e−2	3e−1	5e−2	7e−1	2e−2	7e−1	5e−2
128	9e−2	3e−3	9e−2	6e−3	2e−1	6e−2	7e−1	9e−3	7e−1	3e−2
256	1e−2	1e−3	4e−2	2e−3	2e−1	6e−2	3e−1	3e−3	3e−1	2e−2
$\Delta = .75$										
32	7e−1	3e−2	7e−1	5e−2	7e−1	7e−2	7e−1	7e−2	7e−1	7e−2
64	7e−1	3e−2	7e−1	5e−2	7e−1	7e−2	7e−1	7e−2	7e−1	7e−2
128	7e−1	5e−3	7e−1	5e−2	7e−1	7e−2	7e−1	7e−2	7e−1	7e−2
256	2e−2	2e−3	3e−2	3e−3	7e−1	7e−2	7e−1	6e−3	4e−1	3e−2

Table 3
Stable step size for the first-order explicit scheme. Simulation parameters and the initial configuration of the vesicle are the same as the simulation shown in Fig. 3.

n	$v = .1$		$v = 1$		$v = 10$	
	$\chi = 1$	10	1	10	1	10
32	3e−4	2e−4	2e−3	1e−3	3e−3	1e−3
64	2e−5	2e−5	9e−5	1e−4	2e−4	2e−4
128	2e−6	3e−6	3e−6	5e−6	1e−5	2e−5
256	3e−7	2e−7	6e−7	3e−7	2e−6	1e−6

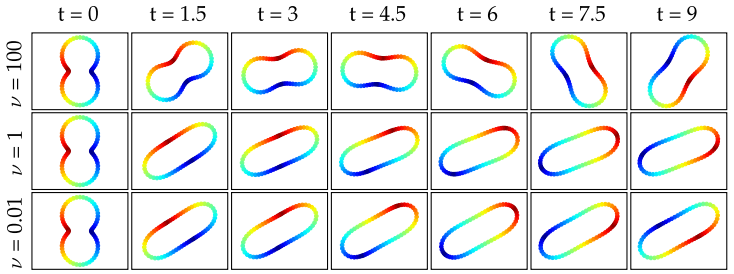

Fig. 3. The evolution of a single vesicle in an unbounded shear flow. The viscosity contrast $\nu = .01$, 1, and 100, $\chi = 1$, $\kappa_b = 1$, reduced area $\Delta = .75$, and time horizon $T = 9$. Lagrangian points on the vesicle membrane is colored for visual purposes only and has no other significance. When $\nu < \nu_c$ we see that the vesicle reaches an equilibrium and then undergoes tank-treading motion (see Fig. 6 for further analysis). When ν is large the vesicle tumbles.

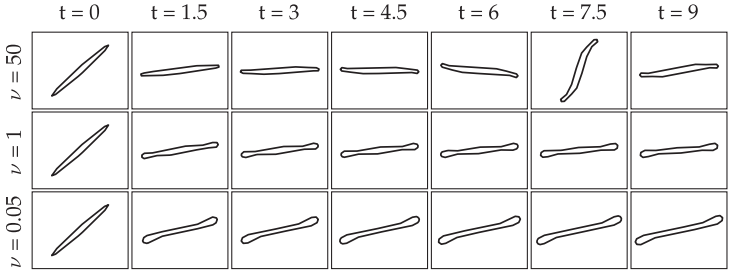

Fig. 4. The same as Fig. 3 with the reduced area $\Delta = 0.2$.

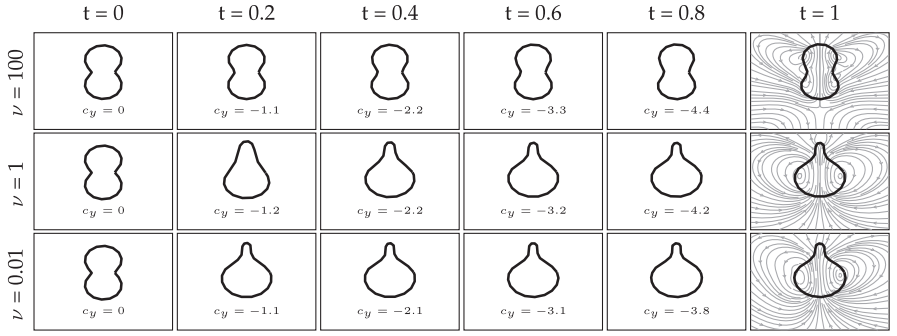

Fig. 5. Here we depict the sedimentation shape of a vesicle for different viscosity contrasts. The viscosity contrast $\nu = .01$, 1, and 100, $\kappa_b = 1$, reduced area $\Delta = .75$, $\Delta\rho = 1$, $\mathbf{g} = -40\mathbf{e}_y$, and time horizon $T = 1$.

viscosity contrasts larger than that, the vesicle starts to tumble. For $\nu < \nu_c$, there exists an angle β_ν in which the vesicle tank-treads. We investigate the dependence of the inclination angle β_ν (defined below) of a vesicle with reduced area $\Delta = .75$. We stopped the simulation when the rate of change in the inclination angle was less than one percent of the its value, i.e. $\left|\frac{1}{\beta}\frac{d\beta}{dt}\right| \leqslant .01$. The alignment of the vesicle with the flow increases as the viscosity contrast is increased. A viscosity difference of $\nu_c \approx 4.1$ is the fold bifurcation point. Vesicles with larger viscosity difference undergo tumbling. As we further increase the viscosity contrast, the frequency of tumbling increases. However, we did not investigate the effect of parameters on the frequency of tank-treading and tumbling motions. Our stopping criteria explain the slight decrease in the dependence of β_ν versus the shear rate χ.

We define the inclination angle as the angle between the principal axis corresponding to the smallest principal moment of inertial with the x_1-axis. We calculate the moment of inertia tensor J by

$$J = \int_\omega (|\mathbf{r}|^2 I - \mathbf{r}\otimes\mathbf{r})d\mathbf{x} = \frac{1}{4}\int_\gamma \mathbf{r}\cdot\mathbf{n}(|\mathbf{r}|^2 I - \mathbf{r}\otimes\mathbf{r})ds,$$

where $\mathbf{r} = \mathbf{x} - \mathbf{c}$ is the distance of point $\mathbf{x}$ from the centroid $\mathbf{c}$. The principal axes of inertia are the eigenvectors of J.

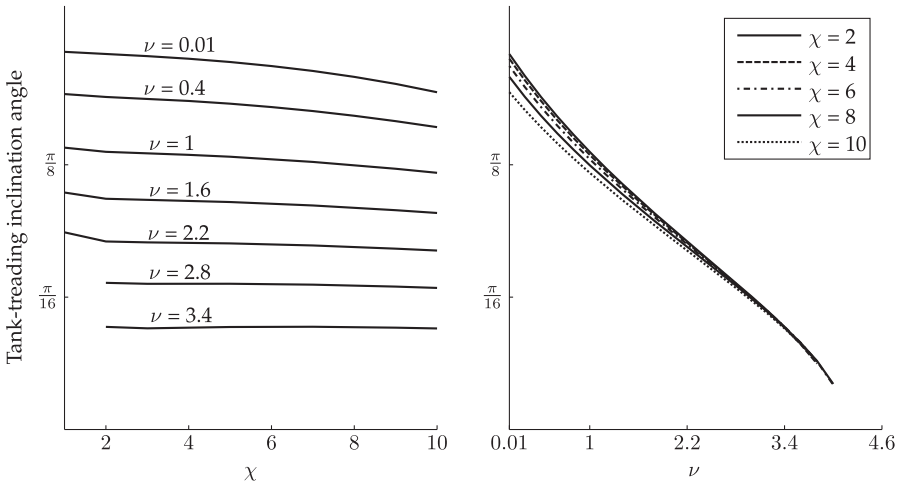

Fig. 6. For small values of viscosity contrast, a vesicle reaches steady-state and then undergoes a motion called tank-treading (see the bottom row of plots in Fig. 3). Theory and experiment suggest that the inclination angle of the vesicle during tank-treading depends solely on the viscosity contrast ν and the reduced area Δ; this dependence is confirmed in our computations. Here, the reduced area $\Delta = .75$. The critical value for viscosity contrast is $\nu_c \approx 4.1$.

Table 4
Number of GMRES iteration averaged over 100 time steps. The time horizon $T = 2/\chi$ (and *10* when $\chi = 0$), $\kappa = 1$, and $\Delta = .75$. GMRES tolerance is set to 10^{-8} for the position solver and 10^{-12} for tension solver. The extrapolated position is used as starting point for the GMRES. The preconditioners are the Fourier spectrum of the involved operator on the unit circle [34].

n	$\nu = .01$			$\nu = .1$			$\nu = 1$			$\nu = 10$			$\nu = 100$		
	$\chi = 0$	1	10	0	1	10	0	1	10	0	1	10	0	1	10
Position solver without preconditioner															
32	13	19	13	11	18	10	8	14	7	6	10	7	5	8	8
64	17	35	21	17	34	20	19	29	15	14	20	11	7	12	8
128	41	82	49	43	81	46	47	72	34	34	48	23	16	27	13
256	103	194	122	108	193	116	119	178	84	85	120	55	40	64	31
Position solver with bending spectrum as preconditioner															
32	14	23	21	11	23	16	11	18	12	8	10	8	4	8	6
64	11	25	25	11	25	22	13	20	15	9	11	8	4	8	7
128	13	28	26	13	28	23	14	22	17	10	12	9	4	10	7
256	14	32	29	14	32	25	15	25	18	10	13	9	4	10	8
Preconditioned tension solver															
32	16	17	16	16	17	15	15	16	13	10	13	12	10	12	12
64	18	19	19	18	19	19	18	18	19	16	17	15	12	14	14
128	21	21	21	21	21	21	21	21	21	19	20	18	15	17	17
256	22	22	22	22	22	22	22	22	22	20	21	20	17	20	20

Table 5
The error in area $e_A^n := |A - A_0|/A_0$ and length $e_L^n := |L - L_0|/L_0$ in the evolution of a single vesicle in an unbounded shear flow with shear rate, χ, of 10 and 250. Time marching scheme is chosen to be second-order. Due to inextensibility and incompressibility, the area and length should be preserved. For these tests, $\kappa_b = 1$, $\Delta = .75$, time horizon $T = 1/\chi$, and time step is set to $t_s = T/n$. At low shear rates we observed an erratic convergence behavior also noticed in [14,33,34].

n	$\nu = .04$		$\nu = 1$		$\nu = 25$	
	$e_A^n(e_A^n/e_A^{n-1})$	$e_L^n(e_L^n/e_L^{n-1})$	$e_A^n(e_A^n/e_A^{n-1})$	$e_L^n(e_L^n/e_L^{n-1})$	$e_A^n(e_A^n/e_A^{n-1})$	$e_L^n(e_L^n/e_L^{n-1})$
$\chi = 10$						
32	2.49e−2	2.32e−5	3.66e−4	1.97e−4	3.66e−4	1.97e−4
64	6.26e−3 (3.98)	3.24e−4 (0.07)	8.70e−5 (4.20)	1.31e−4 (1.49)	8.70e−5 (4.20)	1.31e−4 (1.49)
128	1.56e−3 (3.99)	1.31e−4 (2.46)	2.11e−5 (4.11)	5.60e−5 (2.35)	2.11e−5 (4.11)	5.60e−5 (2.35)
256	3.92e−4 (3.99)	4.78e−5 (2.74)	5.23e−6 (4.04)	1.83e−5 (3.04)	5.23e−6 (4.04)	1.83e−5 (3.04)
$\chi = 250$						
32	8.79e−04	2.46e−02	2.97e−06	1.75e−04	2.39e−04	1.73e−04
64	1.56e−04 (5.62)	6.16e−03 (3.99)	4.50e−05 (0.07)	3.16e−05 (5.56)	1.15e−05 (20.7)	3.13e−05 (5.54)
128	2.31e−05 (6.76)	1.50e−03 (4.09)	7.69e−06 (5.85)	8.56e−06 (3.69)	3.02e−06 (3.81)	6.59e−06 (4.75)
256	3.69e−06 (6.26)	3.72e−04 (4.05)	1.36e−06 (5.66)	2.23e−06 (3.83)	6.73e−07 (4.50)	1.50e−06 (4.39)

Table 6
Stable step size for a second-order semi-implicit scheme of two vesicles in shear flow. Both vesicles have reduced area $\Delta = .75$. Snapshots of the flow with $v = 1$ are shown in the plot.

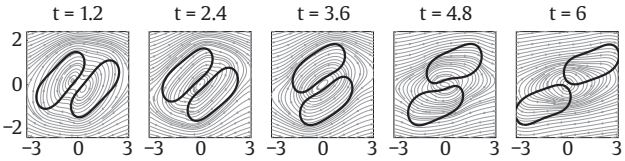

n	$v = .01$		$v = .1$		$v = 1$		$v = 10$		$v = 100$	
	$\chi = 1$	10	1	10	1	10	1	10	1	10
32	7e−1	3e−2	7e−1	5e−2	7e−1	7e−2	4e−1	5e−2	1e−3	5e−4
64	7e−1	3e−2	7e−1	5e−2	7e−1	7e−2	4e−1	4e−2	7e−3	1e−3
128	5e−2	5e−3	1e−1	1e−2	7e−1	7e−2	3e−1	3e−2	1e−2	1e−3
256	1e−2	1e−3	2e−2	2e−3	7e−1	7e−2	2e−1	9e−4	1e−2	1e−3

4.2. Multiple vesicles

First, let us briefly investigate the numerical properties of our scheme in the case of multiple vesicles. In Table 6, we report the stable time-step in the presence of multiple vesicles. The vesicle-flow parameters used in Table 6 remain the same as those in Table 2. For most viscosity contrasts, the stable time-step size is similar to that of a single vesicle. However, for $v = 100$, we observe an order of magnitude smaller time-steps. This time-step growth was expected, if we consider the fact that we use the viscosity of the suspending fluid for scaling and thus when $v = 100$, vesicles behave as rigid bodies, which thus, require smaller time steps in order to resolve their dynamics.

The collision of deformable particles has received substantial attention in the literature. From one aspect, the particle–particle interactions in a suspension will produce irregular motions one of which is the lateral migration of particles. This migration causes dispersion in the suspension. Eckstein et al. [7] discussed the importance of this phenomena and performed experiments involving rigid particles. Loewenberg and Hinch [16] performed a numerical study of the collision of two deformable drops in shear flow.

Here, we investigate the effect of vesicles' viscosity contrast on their lateral migration in an unbounded shear flow. Initially one of the vesicles is located at the origin and the other one at $[-10,.5]^T$. The shear rate $\chi = 2$ and vesicles' bending modulus κ_b is chosen to be 0.1. The relative orientation of vesicles is a factor in the dynamics of collision and a statistical approach is needed to study its effect. Here, to minimize the effect of vesicles' orientation we choose the vesicle be very close to a circle with reduced area $\Delta = .98$. We define the offset between two vesicles to be $\delta := |c_{y,1} - c_{y,2}|$, where $c_{y,i}$ is the y coordinate position of ith vesicle's centroid ($i = 1,2$).

In Fig. 7, snapshots of the interaction between vesicles are shown. Due to the inextensibility of a vesicle's membrane and the incompressibility of its fluid, vesicles maintain their circular shape at all times. In the last column of Fig. 7, we plot the streamlines at an intermediate time.

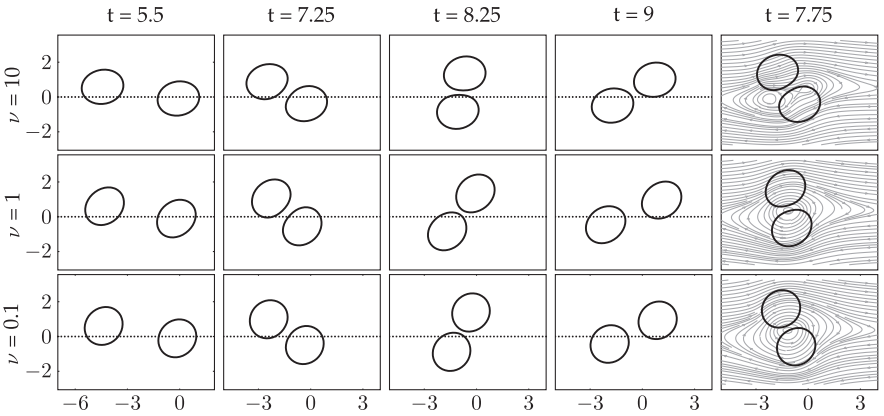

Fig. 7. Snapshots of the position of two vesicles in shear flow. Initially, one of the vesicles is located at the origin and the other one at $[-10,.5]^T$. To minimize the effect of relative orientation of vesicles on the dynamics of collision we choose the vesicles to be two identical ellipsoids with $\Delta = .98$ and $\kappa_b = .1$. In the last column we plot the streamlines at an intermediate time $t = 7.75$. Each row corresponds to a different viscosity contrast v. The offset between the centroids of the vesicles is plotted in Fig. 8.

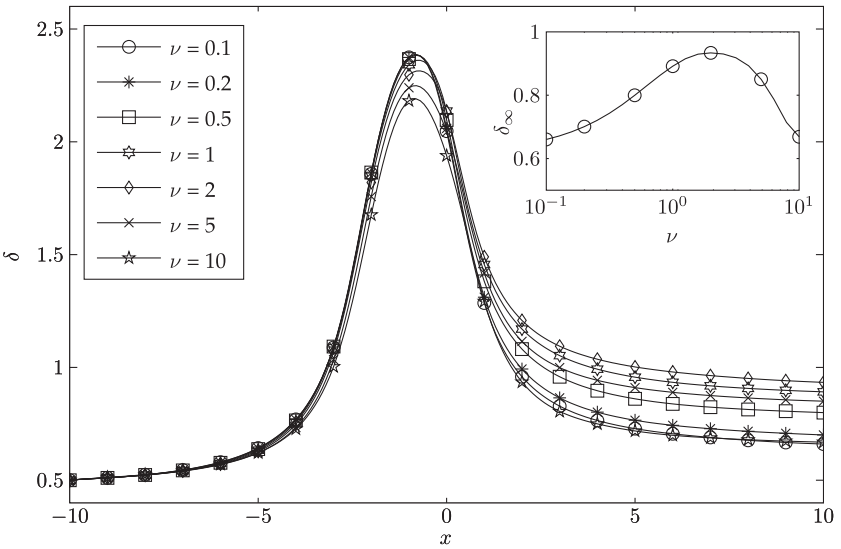

Fig. 8. The offset δ between the centroids of two vesicles in shear flow. A few exemplary snapshots of interacting vesicles are plotted in Fig. 7. In the inset, the offset of the vesicle at $x = 10$, denoted by δ_∞, is plotted versus viscosity contrast v.

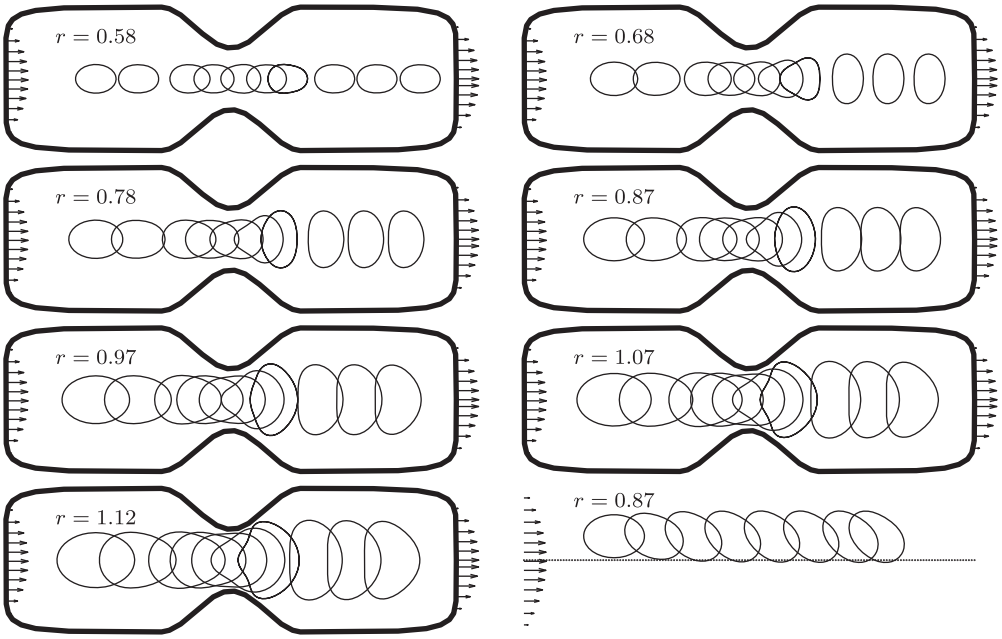

Fig. 9. Here, we depict the shape of a evolution of a single vesicle in a constricted tube. Each subplot corresponds to a different vesicle size: r denotes the relative size of the vesicle with respect to diameter of the tube (defined in the text). A Poiseuille flow boundary condition on the inlet and outlet of the tube is prescribed (vector plot). In order to investigate, the error incurred due to explicit treatment of the walls, we repeat a "similar" test without boundaries, in which we offset the initial position of vesicle by *1*. This experiment is depicted in the bottom-right plot. In all of the experiments, $v = 1$ and $\kappa_b = .5$.

In Fig. 8, we plot the offset δ versus x for different values of viscosity contrast v. The qualitative dependence of the offset on position is the same. However, we can see in the inset, the final offset δ_∞ does not monotonically depend on v. Initially, by increasing the viscosity contrast, the final offset increases. But as v becomes larger than one, the offset starts to decrease. The decrease in the final offset value when $v \gg 1$ is expected because the vesicle behaves increasingly like a rigid particle in which case the Stokes flow is reversible. However, the initial increase comes as a surprise. This trend is in contrast with the monotone decrease of the final offset for bubbles [16]. In a separate paper, different aspects of the dynamics of vesicle collision and dispersion will be considered.

4.3. Vesicles in confined domains

The main question in the confined geometry case concerns the numerical stability of our scheme, which treats vesicle-boundary interaction explicitly. To examine the stability of our scheme, we consider the flow of a vesicle in a constricted tube. On the fixed boundaries, we impose velocity boundary conditions that correspond to an unperturbed Poiseuille flow.

In this experiment, we consider three cases with viscosity contrasts .04, 1 and 25, respectively, and $\kappa_b = .5$. There are 400 grid points on the fixed boundary and 128 points on the vesicle. The initial shape of the vesicle is an ellipsoid with reduced area $\Delta = .94$. We increase the size of the vesicle compared to the opening of the channel, and monitor the error. As a measure of the relative size, we set $r := (a + b)/2c$, where a and b are, respectively, major and minor diameter of vesicle and c is the size of the gap in the tube. To have an estimate on the errors in case of unbounded flow (and thus being able to distinguish the effect of the walls), we also simulate the evolution of a single vesicle in unbounded Poiseuille flow. We report the errors in Table 7. Also observe that in case of unbounded Poiseuille flow, the vesicle starts to migrate toward the center line. This phenomenon was studied in detail in [11].

In Table 7 we compare the stable step size corresponding to the second-order time-stepping scheme of bounded flow with that of an unbounded Poiseuille flow. For the case of a vesicles with small viscosity contrast ($\nu = .2$), their faster time scale makes them responsive to the sudden outward flow in the divergent part of the tube and therefore for large vesicles, time steps should be chosen such that the vesicle does not cross the boundary of the domain.

4.4. Rheology of a suspension

In this section, we discuss numerical homogenization for suspension rheology. The effective viscosity of a suspension can be defined as the viscosity of a homogeneous Newtonian fluid that has the same energy dissipation per macroscopic volume element. We derive the effective viscosity as the constant of proportionality between rates of energy dissipation with and without the inclusions. This definition coincides with the one derived by averaging the stress over a volume for particulate flows [9]. In Appendix B, we give a brief derivation of average stress tensor in a vesicle suspension (see Table 8).

For dilute suspensions, the particle–particle interactions are negligible and the effective stress can be written in terms of flow past an isolated or *"reference"* vesicle [3,4]. In simple shear flow, the ambient velocity field is given by $\mathbf{u}(x,y) = [\chi y, 0]^T$, where χ is the shear rate. For a suspension of vesicles in such a flow, we define

$$[\mu] := \frac{\mu_{\text{eff}} - \mu_0}{\phi \mu_0} = \frac{1}{\chi \mu_0 T} \int_{T_i}^{T_e} \langle \sigma^p_{12} \rangle dt, \tag{4.1}$$

in which,

$$\langle \sigma^p \rangle = \frac{1}{|\omega|} \int_\gamma [\zeta \otimes \mathbf{x} + \mu_0 (\nu - 1)(\mathbf{u} \otimes \mathbf{n} + \mathbf{n} \otimes \mathbf{u})] ds, \tag{4.2}$$

where $[\mu]$ is referred to as the "intrinsic viscosity", ϕ is the areal contrast of vesicles, σ^p is the perturbation in the stress due to presence of vesicles and $\langle \cdot \rangle$ is the spatial average (see Appendix B for its derivation). T_i is the point at which we start the

Table 7
In this table we report errors in area $e_A := |A - A_0|/A_0$ and length $e_L := |L - L_0|/L_0$ for the simulation in Fig. 9. For values of $r > 1.25$ a vesicle with $\Delta = .94$ is larger that the gap and cannot pass though it (due to inextensibility and incompressibility).

		Unbounded	r (contrast of vesicle's representative length to the size of the opening)						
		($r = .87$)	.58	.68	.78	.87	.97	1.07	1.12
$\nu = .2$	e_A	4.73e−4	1.29e−4	1.30e−4	1.17e−4	8.02e−5	3.18e−5	3.57e−4	1.90e−4
	e_L	1.95e−4	2.58e−4	2.47e−4	2.41e−4	2.39e−4	2.42e−4	1.93e−4	1.97e−4
$\nu = 1$	e_A	6.65e−4	7.13e−3	2.19e−4	3.69e−4	4.17e−4	4.27e−4	4.30e−4	2.98e−3
	e_L	4.72e−4	9.89e−5	5.25e−4	8.21e−4	9.33e−4	1.05e−3	1.19e−3	1.23e−3
$\nu = 5$	e_A	2.78e−4	2.85e−5	2.02e−6	6.45e−6	1.46e−5	4.35e−5	1.89e−4	2.67e−4
	e_L	1.03e−4	7.17e−4	2.98e−4	1.68e−4	1.05e−4	1.43e−4	1.69e−4	1.95e−4

Table 8
Stable step size for a second-order semi-implicit scheme of a vesicle in a constricted tube compared to that of the unbounded Poiseuille flow.

n	Unbounded ($r = .87$)			$r = .87$			$r = 1.12$		
	$\nu = .2$	1	5	.2	1	5	.2	1	5
32	7e−1	7e−1	7e−1	7e−1	7e−1	7e−1	6e−3	7e−1	7e−1
64	7e−1	7e−1	7e−1	7e−1	7e−1	7e−1	1e−2	7e−1	7e−1
128	7e−1	7e−1	7e−1	7e−1	7e−1	7e−1	3e−2	7e−1	7e−1
256	7e−1	7e−1	7e−1	7e−1	7e−1	7e−1	9e−3	7e−1	7e−1

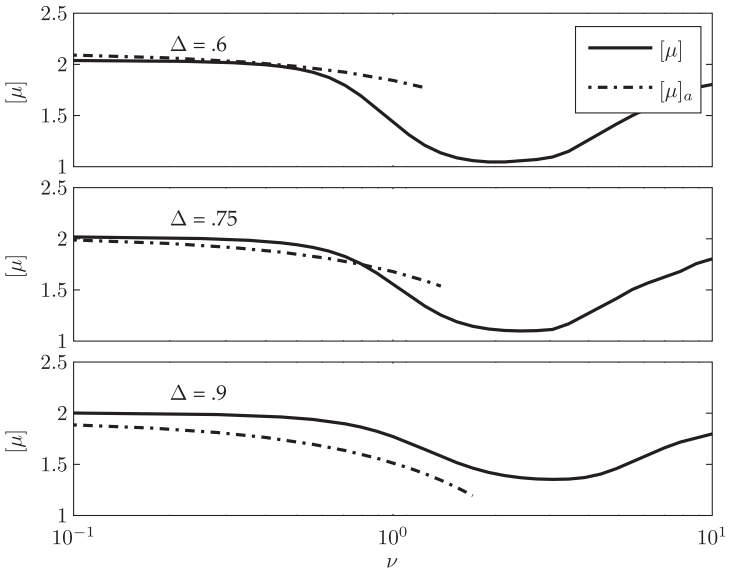

Fig. 10. The intrinsic viscosity of the homogeneous fluid vs. viscosity contrast of the suspension for different values of reduced area Δ. As we increase v, the vesicles align with the flow and the intrinsic viscosity decreases. When $v > v_c$, tumbling occurs and the reference vesicle does not maintain a fixed orientation. The frequency of this tumbling motion is inversely proportional to v_c: as we increase v, vesicles tumble faster, which in turn causes an increase in the intrinsic viscosity $[\mu]$.

measurement and is chosen such that the reference vesicle has reached a steady-state (for $v < v_c$), T_e is the end of simulation, and $T = T_e - T_i$. In our formulation, the traction jump across the interface is given by $\zeta = \mathbf{f}_b + \mathbf{f}_\sigma = -\kappa_b \mathbf{x}_{ssss} + (\sigma \mathbf{x}_s)_s$. Using integration by parts, we obtain

$$\int_\gamma \zeta \otimes \mathbf{x} ds = -\int_\gamma (\kappa_b \kappa^2 \mathbf{n} \otimes \mathbf{n} + \sigma \mathbf{t} \otimes \mathbf{t}) ds. \tag{4.3}$$

As a validation of our scheme, in Fig. 10 we report the intrinsic viscosity for a dilute suspension of vesicles in simple shear flow. The vesicle is an ellipse with reduced area $\Delta = .75$ and bending modulus of 1. When $0 < v < v_c$, the vesicle tank-treads. Larger values of v cause the vesicle to align itself with the flow thus resulting in less resistance. On the onset of tumbling, we observe that the intrinsic viscosity increases.

Misbah [18] derived an analytical expression for the effective viscosity of a suspension of quasi-spherical vesicles in the tank-treading region. According to [18], we have

$$[\mu]_a := \frac{5}{2} - \frac{(23v + 32)\Delta}{16\pi}. \tag{4.4}$$

The dashed line in Fig. 10, corresponds to $[\mu]_a$ obtained from this formula. The qualitative agreement between the analytical result for quasi-spherical vesicles and our numerical simulations for 2D vesicles is good. To our knowledge, there is no analysis for the case of a tumbling motion.

5. Conclusions

We proposed a semi-implicit numerical scheme to simulate the motion of inextensible vesicles suspended in bounded or unbounded domains. For several test-cases, we have demonstrated, through the use of numerical experiments, that the proposed scheme does not exhibit a mesh-dependent high-order stability constraint on the time-step size. Our scheme exhibits second-order accuracy in time and spectral-accuracy in space. We have presented efficient low-cost preconditioners to solve the discrete evolution equations by iterative solvers. An additional extension of our work would be to design an algorithm that allows decoupling of the time-step size from the shear rate. We believe, however, that such an algorithm would require the use of nonlinear solvers and contact detection methods that fully couple the vesicle position updates. Such coupling would be more difficult to implement and analyze. Our next step will be the extension of this scheme in three dimensions.

Appendix A. Completed indirect solution of Stokes flow in a confined geometry

Consider the domain Ω given in Section 2 in the absence of vesicles. The solution of the Stokes Eq. (2.1a) in this domain can be written as a double-layer integral with density $\boldsymbol{\eta}$ [20,23]. The velocity and pressure at a point $\mathbf{x} \in \Omega$ can be written as

$$\mathbf{u}(\mathbf{x}) = \mathcal{D}[\mathbf{y},\boldsymbol{\eta}](\mathbf{x}) = \frac{1}{\pi}\int_\Gamma \frac{\mathbf{r}\cdot\mathbf{n}}{\rho^2}\frac{\mathbf{r}\otimes\mathbf{r}}{\rho^2}\boldsymbol{\eta}ds, \tag{A.1}$$

$$p(\mathbf{x}) = \mathcal{K}[\mathbf{y},\boldsymbol{\eta}](\mathbf{x}) = -\frac{\mu}{\pi}\int_\Gamma \frac{\mathbf{n}\cdot\boldsymbol{\eta}}{\rho^2} - 2\frac{\mathbf{r}\cdot\mathbf{n}}{\rho^2}\frac{\mathbf{r}\cdot\boldsymbol{\eta}}{\rho^2}ds. \tag{A.2}$$

As it is nicely explained in [12], Eq. (A.1) cannot represent general flow fields. In particular, it cannot represent the flow due to rigid body motions. To compensate for this deficiency, following [20], we add *Stokeslet* and *Rotlet* terms for each $\Gamma_k (1 \leqslant k \leqslant M)$ to Eq. (A.1). The Stokeslet is the Green's function for the Stokes equation, which is the same as the single-layer kernel S given in (2.5). The Rotlet is the antisymmetric component of the Stokes doublet defined by

$$R(\mathbf{x},\mathbf{y})(\xi) := \frac{\xi}{\mu}\frac{\mathbf{r}^\perp}{\rho^2}, \tag{A.3}$$

for any strength ξ. For a vector $\mathbf{r}$, we define $\mathbf{r}^\perp = (r_1, r_2)^\perp := (r_2, -r_1)$. Both the Stokeslet and Rotlet are centered at an interior point $\mathbf{c}_k$ of the domain enclosed by the boundary component Γ_k. For convenience, we choose $\boldsymbol{\lambda}$, the strength vector for each Stokeslet, and ξ to depend linearly on the unknown density $\boldsymbol{\eta}$ in the following manner:

$$\boldsymbol{\lambda}_{k,1} := \frac{1}{2\pi}\int_{\Gamma_k}\boldsymbol{\phi}_1(\mathbf{y})\cdot\boldsymbol{\eta}(\mathbf{y})ds(\mathbf{y}), \quad \boldsymbol{\lambda}_{k,2} := \frac{1}{2\pi}\int_{\Gamma_k}\boldsymbol{\phi}_2(\mathbf{y})\cdot\boldsymbol{\eta}(\mathbf{y})ds(\mathbf{y}), \tag{A.4}$$

and

$$\xi_k := \frac{1}{2\pi}\int_{\Gamma_k}\boldsymbol{\phi}_3(\mathbf{y})\cdot\boldsymbol{\eta}(\mathbf{y})ds(\mathbf{y}), \tag{A.5}$$

where $\boldsymbol{\phi}_1 = \delta_{1i}$, $\boldsymbol{\phi}_2 = \delta_{2i}$ ($i = 1, 2$) are the rigid body translations in the plane and $\boldsymbol{\phi}_3$ is the rigid body rotation, that is $\boldsymbol{\phi}_3(\mathbf{x}) = \mathbf{x}^\perp$.

Since the flow is confined by the contour Γ_0, as noted in [12,23], conservation of mass (div $\mathbf{u} = 0$) implies that the velocity field defined by (A.1) satisfies the Stokes equation only when $\boldsymbol{\eta}$ satisfies $\int_{\Gamma_0}\boldsymbol{\eta}\cdot\mathbf{n}ds = 0$. To enforce this orthogonality condition, we follow [12] and add an additional operator $\mathcal{N}_0[\mathbf{y},\boldsymbol{\eta}](\mathbf{x}) = \int_{\Gamma_0} N_0(\mathbf{x},\mathbf{y})\boldsymbol{\eta}(\mathbf{y})\,ds(\mathbf{y})$ with kernel $N_0(\mathbf{x},\mathbf{y}) = \mathbf{n}(\mathbf{x})\otimes\mathbf{n}(\mathbf{y})$ to the right-hand side of (A.1). Hence, the velocity for $\mathbf{x}\in\Omega$ can be represented by

$$\mathbf{u}(\mathbf{x}) = \mathcal{D}[\mathbf{y},\boldsymbol{\eta}](\mathbf{x}) + \mathcal{N}_0[\mathbf{y},\boldsymbol{\eta}](\mathbf{x}) + \sum_{k=1}^{M} R(\mathbf{x},\mathbf{c}_k)\xi_k + \sum_{k=1}^{M} S(\mathbf{x},\mathbf{c}_k)\boldsymbol{\lambda}_k =: \mathcal{B}[\boldsymbol{\eta},\Xi,\Lambda](\mathbf{x}), \tag{A.6}$$

where $\Xi = \{\xi_1,\ldots,\xi_M\}$, $\Lambda = \{\boldsymbol{\lambda}_1,\ldots,\boldsymbol{\lambda}_M\}$. In this way, we obtain a system of Fredholm integral equations of the second kind. Taking the limit of (A.6) to points $\mathbf{x}$ on the boundary of the domain, we obtain an equation for $\boldsymbol{\eta}$ supplemented with (A.4) and (A.5) for calculation of $\boldsymbol{\lambda}_k$ and ξ_k

$$\mathbf{U}(\mathbf{x}) = -\frac{1}{2}\boldsymbol{\eta}(\mathbf{x}) + \mathcal{B}[\boldsymbol{\eta},\Xi,\Lambda](\mathbf{x}) \quad \mathbf{x}\in\Gamma, \tag{A.7a}$$

$$\boldsymbol{\lambda}_k = \frac{1}{2\pi}\int_{\Gamma_k}\boldsymbol{\eta}(\mathbf{y})ds(\mathbf{y}), \quad \xi_k = \frac{1}{2\pi}\int_{\Gamma_k}\boldsymbol{\phi}_3(\mathbf{y})\cdot\boldsymbol{\eta}(\mathbf{y})ds(\mathbf{y}). \tag{A.7b}$$

Along with $\boldsymbol{\eta}$, we need the jumps at the boundaries to be able to evaluate the pressure and stress. We have

$$[\![\mathbf{u}]\!] = \boldsymbol{\eta}; \quad [\![p]\!] = -2\mu(\boldsymbol{\eta}_s\cdot\mathbf{t}); \quad [\![\sigma\mathbf{n}]\!] = 0,$$

in which $\mathbf{t}$ is the tangent vector to the boundary, $\boldsymbol{\eta}_s$ denotes the derivative of density with respect to the arc length, and σ is the stress tensor on the boundary.

Appendix B. Average stress in a suspension of vesicles

Consider a suspension of vesicles in an ambient fluid with viscosity μ_0. Each vesicle has a viscosity contrast ν_p. Let Ω denote an arbitrary volume containing several vesicles; let $\langle\cdot\rangle := \frac{1}{|\Omega|}\int_\Omega\cdot d\mathbf{x}$, and let ω^+ denote the infinitesimally enhanced volume containing vesicles. The average stress tensor $\langle\sigma\rangle$ can be broken into two parts as

$$\langle\sigma\rangle = \frac{1}{|\Omega|}\int_\Omega \sigma d\mathbf{x} = \frac{1}{|\Omega|}\int_{\Omega\setminus\omega^+}\sigma d\mathbf{x} + \frac{1}{|\Omega|}\int_{\omega^+}\sigma d\mathbf{x}. \tag{B.1}$$

By definition $\sigma = -pI + 2\mu D$, where D is the strain rate tensor. Substituting into (B.1), we have

$$\langle\sigma\rangle = \frac{1}{|\Omega|}\int_{\Omega\setminus\omega^+} -pI + 2\mu_0 D d\mathbf{x} + \frac{1}{|\Omega|}\int_{\omega^+}\sigma d\mathbf{x}, \tag{B.2}$$

$$= \frac{1}{|\Omega|}\int_\Omega -pI + 2\mu_0 D d\mathbf{x} + \frac{1}{|\Omega|}\int_{\omega^+}\sigma + pI - 2\mu_0 D d\mathbf{x}, \tag{B.3}$$

Table 9
The backward difference coefficients for pth order accurate backward difference method.

p	β	$\mathbf{x}^o$	$\mathbf{x}^e$
1	1	$\mathbf{x}^n$	$\mathbf{x}^n$
2	3/2	$2\mathbf{x}^n - \frac{1}{2}\mathbf{x}^{n-1}$	$2\mathbf{x}^n - \mathbf{x}^{n-1}$
3	11/6	$3\mathbf{x}^n - \frac{3}{2}\mathbf{x}^{n-1} + \frac{1}{3}\mathbf{x}^{n-2}$	$3\mathbf{x}^n - 3\mathbf{x}^{n-1} + \mathbf{x}^{n-2}$
4	25/12	$4\mathbf{x}^n - 3\mathbf{x}^{n-1} + \frac{4}{3}\mathbf{x}^{n-2} - \frac{1}{4}\mathbf{x}^{n-3}$	$4\mathbf{x}^n - 6\mathbf{x}^{n-1} + 4\mathbf{x}^{n-2} - \mathbf{x}^{n-3}$

using the fact $p = -\mathrm{tr}\,(\sigma)/3$ and the divergence theorem for the second integral we obtain

$$= -\langle p\rangle I + 2\mu_0\langle D\rangle + \frac{1}{|\Omega|}\int_{\partial\omega^+}[\sigma\mathbf{n}\otimes\mathbf{x} - \frac{1}{3}(\sigma\mathbf{n}\cdot\mathbf{x})I - \mu_0(\mathbf{u}\otimes\mathbf{n} + \mathbf{n}\otimes\mathbf{u})]ds. \tag{B.4}$$

For the fluid inside each vesicle, we have div $\sigma = 0$. It follows that:

$$0 = \int_{\partial\omega_p^-}\sigma\mathbf{n}\otimes\mathbf{x}ds - \int_{\omega_p^-}\sigma d\mathbf{x} = \int_{\partial\omega_p^-}\left[\sigma\mathbf{n}\otimes\mathbf{x} - \frac{1}{3}(\sigma\mathbf{n}\cdot\mathbf{x})I - \mu_p(\mathbf{u}\otimes\mathbf{n} + \mathbf{n}\otimes\mathbf{u})\right]ds. \tag{B.5}$$

Taking the limit of (B.4) and (B.5) to γ_p, subtracting the results, and denoting the trace of $-\langle\sigma\rangle/3$ by P, we obtain

$$\langle\sigma\rangle = -PI + 2\mu_0\langle D\rangle + \frac{1}{|\Omega|}\sum_p\int_{\gamma_p}[\zeta\otimes\mathbf{x} - \mu_0(1-\nu_p)(\mathbf{u}\otimes\mathbf{n} + \mathbf{n}\otimes\mathbf{u})]ds. \tag{B.6}$$

Appendix C. Backward difference coefficients

We can use the backward difference method to approximate the derivatives and extrapolate forward. We can write $\frac{d\mathbf{x}}{dt} \approx \frac{\beta\mathbf{x}^{n+1} - \mathbf{x}^o}{\Delta t}$, where the coefficients are given in Table 9.

References

[1] B.K. Alpert, Hybrid gauss-trapezoidal quadrature rules, SIAM Journal on Scientific Computing 20 (1999) 1551–1584.
[2] U.M. Ascher, S.J. Ruuth, B.T.R. Wetton, Implicit-explicit methods for time dependent partial differential equations, SIAM Journal on Numerical Analysis 32 (1995) 797–823.
[3] G.K. Batchelor, An Introduction in Fluid Dynamics, Cambridge University Press, 1970.
[4] G.K. Batchelor, The stress system in a suspension of force-free particles, Journal of Fluid Mechanics 41 (1970) 545–570.
[5] J. Beaucourt, F. Rioual, T. Séon, T. Biben, C. Misbah, Steady to unsteady dynamics of a vesicle in a flow, Physical Review Letter E 69 (1) (2004).
[6] G. Danker, C. Verdier, C. Misbah, Rheology and dynamics of vesicle suspension in comparison with droplet emulsion, Journal of Non-Newtonian Fluid Mechanics 152 (1-3) (2008) 156–167.
[7] E.C. Eckstein, D.G. Bailey, A.H. Shapiro, Self-diffusion of particles in shear flow of a suspension, Journal of Fluid Mechanics 79 (1977) 191–208.
[8] Jonathan B. Freund, Leukocyte margination in a model microvessel, Physics of Fluids 19 (2) (2007).
[9] D.J. Jeffrey, A. Acrivos, The rheological properties of suspensions of rigid particles, AIChE Journal 22 (3) (1976) 417–432.
[10] V. Kantsler, V. Steinberg, Transition to tumbling and two regimes of tumbling motion of a vesicle in shear flow, Physical Review Letters 96 (3) (2006).
[11] B. Kaoui, G.H. Ristow, I. Cantat, C. Misbah, W. Zimmermann, Lateral migration of a two-dimensional vesicle in unbounded Poiseuille flow, Physical Review E 77 (2, Part 1) (2008).
[12] S.J. Karrila, S. Kim, Integral equations of the second kind for stokes flow: direct solution for physical variables and removal of inherent accuracy limitations, Chemical Engineering Communications 82 (1989) 123–161.
[13] M. Kraus, W. Wintz, U. Seifert, R. Lipowsky, Fluid vesicles in shear flow, Physical Review Letter 77 (17) (1996) 3685–3688.
[14] M.C.A. Kropinski, An efficient numerical method for studying interfacial motion in two-dimensional creeping flows, Journal of Computational Physics 171 (2) (2001) 479–508.
[15] M. Loewenberg, Numerical simulation of concentrated emulsion flows, Journal of Fluids Engineering-Transactions of the ASME 120 (4) (1998) 824–832.
[16] M. Loewenberg, E.J. Hinch, Collision of two deformable drops in shear flow, Journal of Fluid Mechanics 338 (1997) 299–315.
[17] P.G. Martinsson, V. Rokhlin, A fast direct solver for boundary integral equations in two dimensions, Journal of Computational Physics 205 (1) (2005).
[18] C. Misbah, Vacillating breathing and tumbling of vesicles under shear flow, Physical Review Letters 96 (2) (2006).
[19] H. Noguchi, D.G. Gompper, Shape transitions of fluid vesicles and red blood cells in capillary flows, Proceedings of the National Academy of Sciences of the United States of America 102 (2005) 14159–14164.
[20] H. Power, The completed double layer boundary integral equation method for two-dimensional stokes flow, IMA Journal of Applied Mathematics 51 (2) (1993) 123–145.
[21] H. Power, G. Miranda, Second kind integral equation formulation of stokes' flows past a particle of arbitrary shape, SIAM Journal of Applied Mathematics 47 (4) (1987) 689–698.
[22] C. Pozrikidis, The axisymmetric deformation of a red blood cell in uniaxial straining stokes flow, Journal of Fluid Mechanics 216 (1990) 231–254.
[23] C. Pozrikidis, Boundary Integral and Singularity Methods for Linearized Viscous Flow, Cambridge University Press, New York, NY, USA, 1992.
[24] C. Pozrikidis, Finite deformation of liquid capsules enclosed by elastic membranes in simple shear flow, Journal of Fluid Mechanics 297 (1995) 123–152.
[25] C. Pozrikidis, Effect of membrane bending stiffness on the deformation of capsules in simple shear flow, Journal of Fluid Mechanics 440 (2001) 269–291.
[26] C. Pozrikidis, Interfacial dynamics for stokes flow, Journal of Computational Physics 169 (2001) 250–301.
[27] J.M. Rallison, A. Acrivos, A numerical study of the deformation and burst of a viscous drop in an extensional flow, Journal of Fluid Mechanics 89 (1978) 191–200.

[28] S. Ramanujan, C. Pozrikidis, Deformation of liquid capsules enclosed by elastic membranes in simple shear flow: large deformations and the effect of fluid viscosities, Journal of Fluid Mechanics 361 (1998) 117–143.
[29] Y. Saad, Iterative Methods for Sparse Linear Systems. Society for Industrial and Applied Mathematics, second ed., Philadelphia, PA, USA, 2003.
[30] E. Sackmann, Supported membranes: scientific and practical applications, Science 271 (1996) 43–48.
[31] U. Seifert, Configurations of fluid membranes and vesicles, Advances in Physics 46 (1997) 13–137.
[32] S. Sukumaran, U. Seifert, Influence of shear flow on vesicles near a wall: a numerical study, Physical Review Letter E 64 (1) (2001).
[33] A. Tornberg, M.J. Shelley, Simulating the dynamics and interactions of flexible fibers in stokes flows, Journal of Computational Physics 196 (1) (2004) 8–40.
[34] S.K. Veerapaneni, D. Gueyffier, D. Zorin, G. Biros, A fast algorithm for hydrodynamic interactions of inextensible vesicles in 2D, Journal of Computational Physics 228 (7) (2009) 2334–2353.
[35] V. Vitkova, M. Mader, B. Polack, C. Misbah, T. Podgorski, Micro-macro link in rheology of erythrocyte and vesicle suspensions, Biophysical Journal 95 (6) (2008) L33–L35.
[36] L. Ying, G. Biros, D. Zorin, A high-order 3D boundary integral equation solver for elliptic PDEs in smooth domains, Journal of Computational Physics 219 (1) (2006) 247–275.
[37] Lexing Ying, George Biros, Denis Zorin, A kernel-independent adaptive fast multipole method in two and three dimensions, Journal of Computational Physics 196 (2) (2004) 591–626.
[38] G.K. Youngren, A. Acrivos, Stokes flow past a particle of arbitrary shape: a numerical method of solution, Journal of Fluid Mechanics 69 (1975) 377–403.
[39] Hua Zhou, C. Pozrikidis, The flow of suspensions in channels: single files of drops, Physics of Fluids A: Fluid Dynamics 5 (2) (1993) 311–324.